Journal of Physical Science, Vol. 32(3), 13–29, 2021

Performance Evaluation of Copper and Stainless-steel Electrodes in Electrical Tomographic Imaging

Adedibu Sunny Akingboye[1,2] and Andy Anderson Bery[1*]

[1]School of Physics, Universiti Sains Malaysia, 11800 Pulau Pinang, Malaysia
[2]Department of Earth Sciences, Adekunle Ajasin University, 001 Akungba-Akoko, Ondo State, Nigeria

[*]Corresponding author: andersonbery@usm.my

Published online: 25 November 2021

To cite this article: Akingboye, A. S. & Bery, A. A. (2021). Performance evaluation of copper and stainless-steel electrodes in electrical tomographic imaging. *J. Phys. Sci.*, 32(3), 13–29. https://doi.org/10.21315/jps2021.32.3.2

To link to this article: https://doi.org/10.21315/jps2021.32.3.2

ABSTRACT: *Geophysicists use electrical methods to investigate and characterise the earth's subsurface geology. This study aims to evaluate the performance of copper and conventional stainless-steel electrodes in subsurface tomographic investigations using electrical resistivity tomography (ERT) and induced polarisation (IP) at two sites in Penang, Malaysia. Site 1 and Site 2 employed profile lengths of 200 m and 100 m, with electrodes spacing of 5.0 m and 2.5 m, respectively. In the results of the final data inversion, it was observed that the ERT and IP tomographic models of Site 1 have the best convergence limits with percentage relative differences (copper as reference model) ranging from –70% to 70%, while Site 2 recorded –8% to 8%. The electrodes performance evaluation showed that population root mean square (RMS) error and population mean absolute percentage error (MAPE) of data points between copper and stainless-steel electrodes yielded large values for Site 1 with values above 28% and that of Site 2 was less than 4%. Hence, copper (good electrical conductivity and non-polarisable) electrodes have improved the quality and quantity of infield data which give low values of population RMS error and population MAPE compared to conventional stainless-steel electrodes, especially for large unit electrode spacing surveys. Most notably, this work has contributed to the understanding of the capability of copper electrodes in providing precise and reliable inversion models for subsurface tomographic investigations in pre- and post-land uses (engineering work), hydrogeology/groundwater, environmental studies, etc.*

Keywords: electrical resistivity tomography, induced polarisation, percentage relative differences, electrodes performance evaluation, land uses

1. INTRODUCTION

Subsurface tomographic imaging using the electrical resistivity tomography (ERT) and induced polarisation (IP) has become increasingly popular to determine the low-frequency resistive and capacitive characteristics of earth materials to resolve the variability of the earth's subsurface geology.[1–5] In recent years, ERT has become widely applicable in small to large-scale geophysical investigations because it is cost-efficient. However, the limiting factor of this method is the ambiguity in its geological interpretation. For example, either an increase in ion content in the water formation, higher water content, or higher clay content in sandy formation can generate a low resistivity anomaly. In such a scenario, the chargeability of the formation from the IP survey could resolve the ambiguity.[6,7]

ERT and IP methods are both affected by lithology, pore fluid chemistry, degree of void spaces, and soil water content. Thus, both methods can be deployed to resolve any geophysical problems. However, the IP method is particularly sensitive to changes caused by the membrane polarisation effect due to the clay in geologic formation or electrode polarisation effect caused by conductive minerals partly due to the electrolytic and electronic current flow as explained by Loke.[8] In light of the above, the choice of electrode selection is a pertinent factor for attenuating noise together with improving the efficiency and resolution of the methods to delineate lateral and vertical structures. For instance, some electrode types such as galvanised iron and aluminium are sensitive to noise as explained by LaBrecque and Daily.[9] However, all electrodes are usable with any arrays within a short period of time as explained by Daily et al.[10] The copper electrode can conduct current faster due to its high electrical conductivity.[11] Thus, making it easier to inject current into the earth. It is rarely used because it is expensive compared to other electrodes. Stainless-steel electrode is relatively cheaper than copper; however, it has lower electrical conductivity property compared to copper.[12]

This study, therefore, employs the conventional stainless-steel electrodes and copper electrodes for the ERT and IP subsurface tomographic imaging at two sites within the Universiti Sains Malaysia, Penang. This study aims to assess the performance of these two electrode types based on their subsurface resolution capacities by comparing the qualities of their datasets and inversion models [root mean square (RMS) errors, total of data points, and percentage of relative differences].

2. LOCATION AND GEOLOGICAL SETTING

The study area is in Minden within the Universiti Sains Malaysia, Penang, Malaysia. Penang is located on the northern side of Peninsular Malaysia. Geologically, Penang is underlain by igneous rock formation, typically granites (Figure 1). The granites of Penang are divided into two main groups namely the North Penang Pluton and the South Penang Pluton, based on the proportion of alkali feldspar to total feldspar. The North Penang Pluton consists of granite, which is rich in orthoclase to intermediate microcline, while the South Penang Pluton is typical of granite with microcline.[13,14]

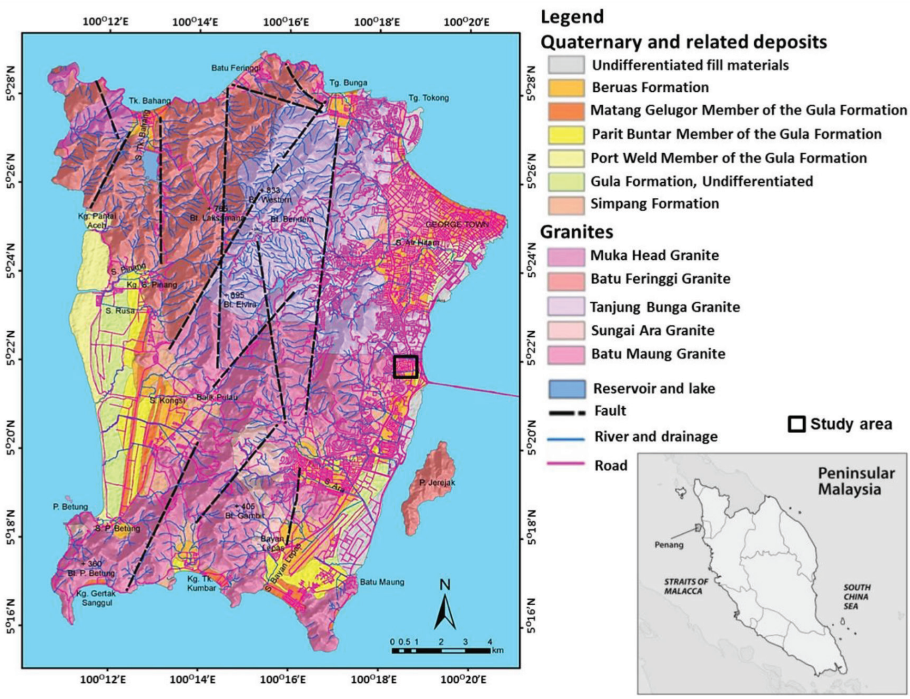

Figure 1: Geological map of Penang, Malaysia showing the study area (modified from Ahmad et al., 2006 and Abdul Hamid et al., 2019).[14,15]

3. EXPERIMENTAL

Two sites were investigated in the study area with only just two traverses. Site 1 traverse falls between latitudes 5°21’43.56”–5°21’44.89” N and longitudes 100°18’20.09”–100°18’26.64” E, while Site 2 runs from 5°21’32.58”–5°21’29.15” N and 100°18’31.32”–100°18’30.86” E. Site 1 employed a survey line of 200 m in length, with a 5.0 m electrode spacing, while Site 2 utilised a total spread length of 100 m with an electrode spacing of 2.5 m. Both sites used the same number of electrodes, with a total of 41 copper and stainless-steel electrodes and the array type used was the Wenner-Schlumberger. The acquisition system was set to record only the positive data points and reject all the negative data points to increase their resolutions as they can produce artefact in the generated tomograms. To have a detailed interpretation of subsurface layers and their depth (maximum of 41 m), a borehole log (Figure 2) derived at station distance of 85 m at Site 1 (the black vertical rectangular bars shown in ERT and IP inverted models) was used to constraint the generated inversion results. The borehole litho-section runs from the ground level to a depth of 41 m. The variation in profile length and electrode spacing was aimed at determining the efficiency of each of the used electrodes. The summary of the survey parameters employed at both sites is tabulated in Table 1 and Figure 3 shows the field image of the survey setups.

Table 1: Summary of the ERT and IP survey parameters employed for the study.

Surveying parameter	**Site 1**	**Site 2**
Tomographic technique	ERT and IP	
Electrode type (6 mm in diameter)	Copper and stainless-steel	
Array type	Wenner-Schlumberger	
Maximum stack	2	
Maximum current output (mA)	200	
Acquisition delay (s)	0.4	
Acquisition time (s)	0.6	
Current-off (s)	1.0	
Total of spread length (m)	200	100
Minimum electrode spacing (m)	5.0	2.5

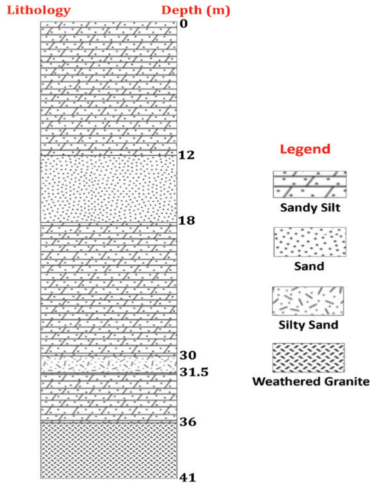

Figure 2: Borehole litho-section traversed at a station distance of 85 m at Site 1.

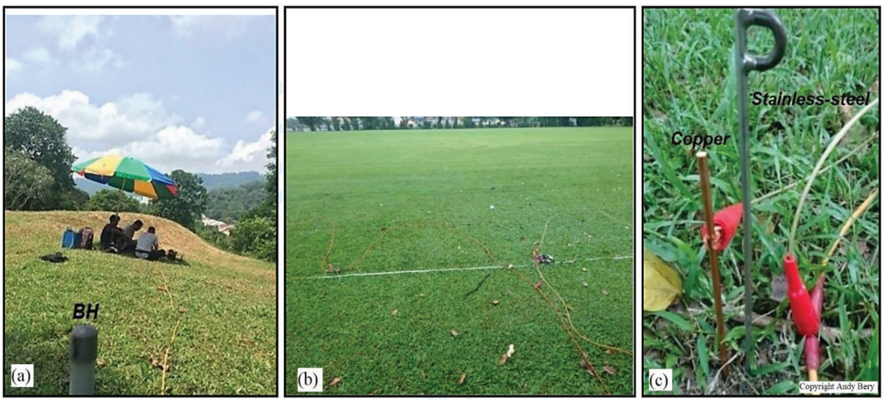

Figure 3: The pictorial view of (a) Site 1 and (b) Site 2 showing a section of the survey profile lines and borehole point indicated as BH at Site 1, while (c) shows the grounded copper electrode (left rod) and stainless-steel electrode (right rod).

Source of images: Author (Andy Bery)

The acquired field datasets for ERT and IP were processed and iteratively inverted using the Res2dinv software (Geotomo Software Sdn Bhd, Penang, Malaysia). This inversion process uses a mathematical inverse problem involving forward modelling and data inversion to determine the true resistivity distribution of the subsurface formation.[8,16] To obtain the finest tomographic model inversion, the finite-element method of 4 nodes with L_2-norm was used as the least-squares constraint to minimise the differences between the calculated and observed apparent resistivity values. Next, a damping factor of 0.05 with a minimum value of 0.01 was employed to increase the accuracy of the calculated apparent resistivity and the resolution of the generated inverted resistivity model sections apart from stabilising the inversion process. In this study, the selected cut-off error was 30% from the maximum error of 200%. Hence, only data points with apparent resistivity percentage errors of 30% and below were used in the final inversion process. This approach was used to avoid creating unrealistic variations in the model interpretation. The number of iterations for the ERT and IP tomograms was limited to seven to make sure the error was converged to the lowest condition. According to Scapozza and Laigre, the optimal model of the subsurface normally reached to seven iterations.[17] However, Loke, and Akingboye and Ogunyele suggested that an inverted tomographic model with the lowest convergence error limit may sometimes not give the required ideal subsurface geological structures and anomalies.[8,18] Based on these facts and critical examinations of the generated RMS errors for iterations from 5th and above, we, therefore, considered the 7th iteration as the ideal one as it yielded significantly no or small changes in error values and at the same time produced the most realistic subsurface inverted ERT and IP models.

To identify the percentage relative changes between the ERT and IP inversion model results, the copper electrodes datasets were set as the reference, as their overall inversion results were proven to be reliable based on the quality of population data points and low RMS errors than that of the conventional stainless-steel electrodes. Hence, equation 1 was used for the analysis of the percentage relative difference. Additionally, three other statistical parameters, namely the population mean (μ) (equation 2), population standard deviation (σ) (equation 3), population RMS error (equation 4), and population mean absolute percentage error (MAPE) (equation 5) were used to evaluate the performance of both electrode types. In statistics, population μ is also called average. The population σ measures the dispersion amount of individual data values from the population μ values, while the population RMS error measures how far the error from 0 on average is. The population MAPE is a statistical measure of how accurate a forecast is. The percentage format in relative difference was used for the statistical analyses in this work to enable the comparison of data with different population sizes and to express the number of changes. These analyses provided a better picture of the performance between the two electrodes in the ERT and IP surveys.

$$X_{\%\text{ relative difference}} = \frac{X_{\text{copper}} - X_{\text{stainless—steel}}}{X_{\text{copper}}} \times 100\% \tag{1}$$

$$\text{Mean }(\mu) = \frac{1}{N}\sum_{i=1}^{N} X_{\%\text{ relative difference }(i)} \tag{2}$$

$$\text{SD }(\sigma) = \sqrt{\frac{\sum_{i=1}^{N}\left(X_{\%\text{ relative difference }(i)} - \mu\right)^2}{N}} \tag{3}$$

$$\text{RMS} = \sqrt{\frac{\sum_{i=1}^{N}\left(X_{\%\text{ relative difference }(i)}\right)^2}{N}} \tag{4}$$

$$\text{MAPE} = \frac{100\%}{N}\sum_{i=1}^{N}\left| X_{\%\text{ relative difference}} \right| \tag{5}$$

where x represents geophysical parameters, namely, resistivity (ohm.m) and chargeability (msec).

4. RESULTS AND DISCUSSION

The ERT and IP inversion results for the stainless-steel and copper electrodes at Site 1 yielded a similar range of resistivity and chargeability values from 10–1800 ohm.m and 1–18 msec, respectively (Figures 4 and 5). Based on their inversion results in terms of RMS errors, the stainless-steel electrodes derived resistivity and chargeability inversion RMS errors of 26.2% and 6.0%, while that of copper electrodes were 14.1% and 1.8%, respectively. Furthermore, by correlating the ERT and IP inversion results (for both stainless-steel and copper electrodes) at Site 1 with the borehole layered sequence, the sandy silt top layer, sandy layer, and silty sand had resistivity values of 70–600 ohm.m, 400–800 ohm.m, and 300–600 ohm.m, respectively. Meanwhile, the chargeability values ranged between 3–5 msec, 1–4 msec, and 1–5 msec for sandy silt top layer, sand layer, and silty sand, respectively. The borehole log (Appendix 1) provided detailed understanding on the nature of the subsurface layers and crustal materials imaged in the ERT and IP models.

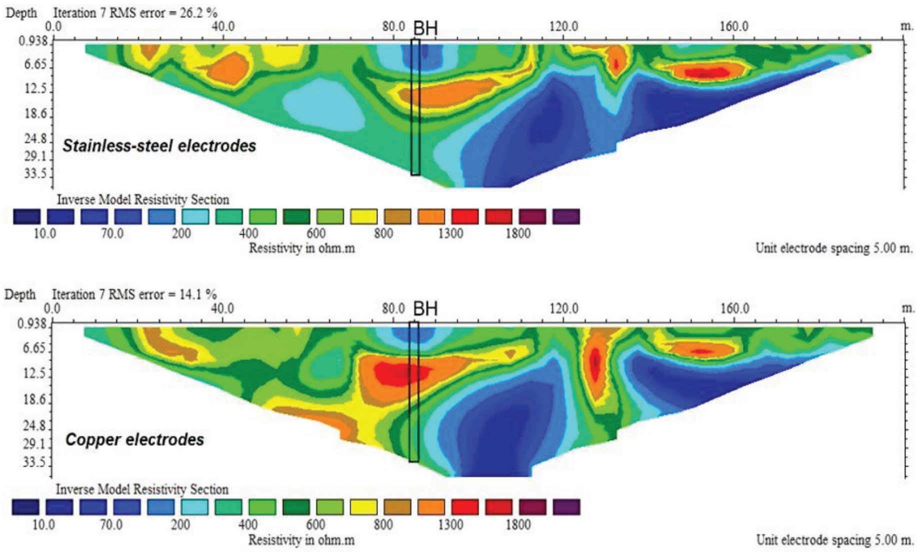

Figure 4: ERT inversion models for Site 1 using stainless-steel and copper electrodes.

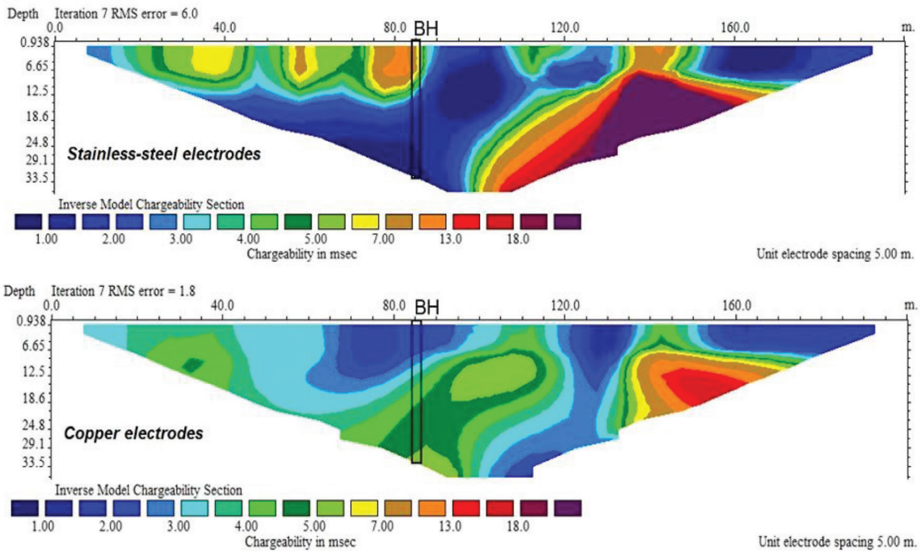

Figure 5: IP inversion models for Site 1 using stainless-steel and copper electrodes.

As for Site 2, the ERT and IP inversion results for the stainless-steel and copper electrodes yielded the same range of resistivity and chargeability values ranging from 50–1200 ohm.m and 1.0–2.6 msec, respectively (Figures 6 and 7). The resistivities of the sandy silt, sand, and silty sand materials ranged from 90–600 ohm.m, 400–800 ohm.m, and 200–600 ohm.m, respectively. On the other hand, the chargeability values obtained from the IP inversion results ranged from 1.4–1.8 msec, 1.6–2.4 msec, and 1.4–2.2 msec for the sandy silt, sand, and silty sand materials, respectively. The RMS errors of the ERT inversion results for both electrode types yielded the same values of 4.5%. However, the IP inversion result indicated a slight variation in the generated RMS errors with values of 0.46% and 0.19% for the stainless-steel and copper electrodes, respectively.

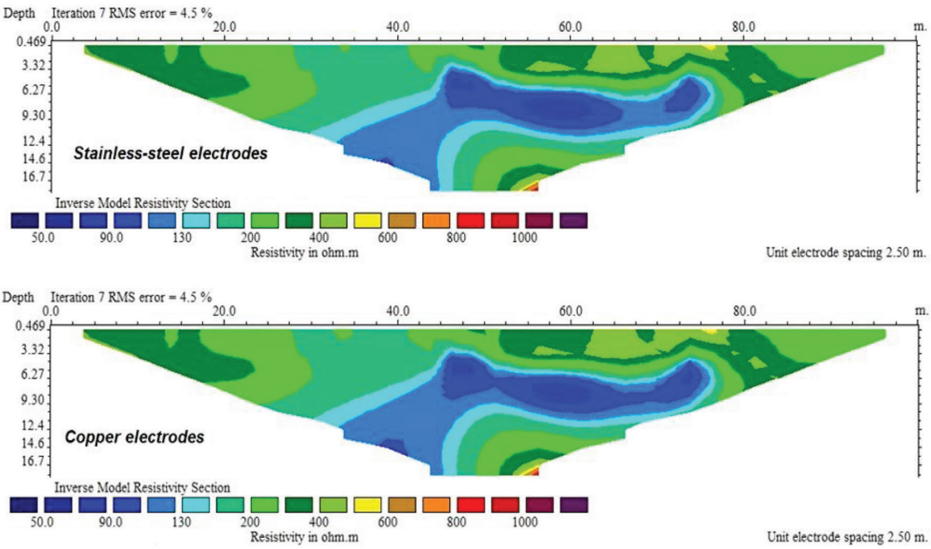

Figure 6: ERT inversion models for Site 2 using stainless-steel and copper electrodes.

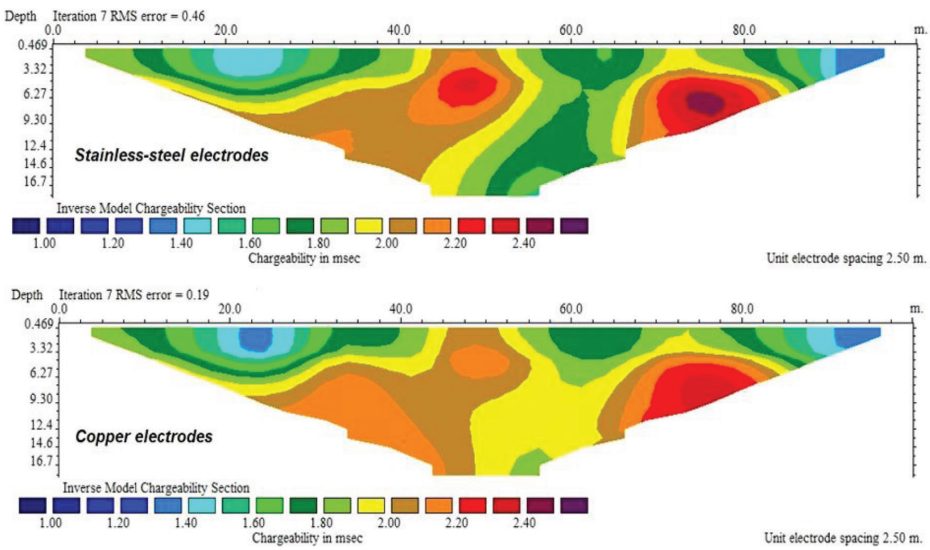

Figure 7: IP inversion models for Site 2 using stainless-steel and copper electrodes.

4.1 Performance Evaluation Between Copper and Stainless-steel Electrodes

To further substantiate the performance ratings of both electrode types used in this study, the RMS errors of the ERT and IP inversion models were plotted against their iteration levels for the two investigated sites. According to Figures 4–7, copper electrodes yielded lower RMS errors than the stainless-steel electrodes for both ERT and IP models. At Site 1, the ERT model RMS errors reduced from 30.20% to 26.04% for the stainless-steel electrodes and 17.79% to 13.74% for the copper electrodes. Meanwhile, at Site 2, the ERT model RMS errors reduced from 6.42% to 4.39% for the stainless-steel electrodes and 6.40% to 4.41% for the copper electrodes. Figure 8 illustrates the percentage relative differences in ERT RMS errors at the 7th iteration between stainless-steel and copper electrodes (12.13% and 0.01% for Site 1 and Site 2, respectively). The RMS errors using stainless-steel doubled that of copper electrodes at Site 1. This is because large electrode spacing requires good material as a conductor to inject and to receive current effectively into the subsurface. In addition, Figure 9 represents the data population quality of generated models in terms of data quality (before and after the filtering process). This statistical result has shown that the copper electrode is more suitable than the conventional stainless-steel electrodes. For example, Sirhan *et al.* used copper electrodes and successfully investigated water resources at West Bank, Palestine.[19] Meanwhile, our statistical results concurred with this previous work and the work conducted by Cardarelli and Di Filippo in Milan which used steel and copper electrodes to improve the IP interpretation results.[20]

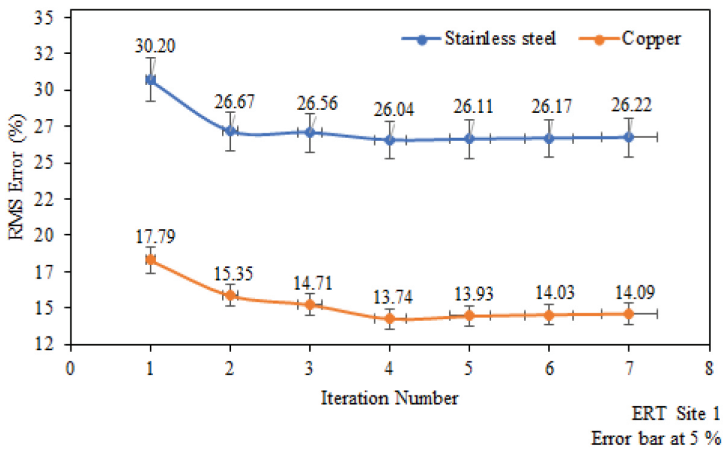

(a)

Figure 8: Graphs of RMS error versus iteration number of ERT inversion models at (a) Site 1 and (b) Site 2 (continued on next page).

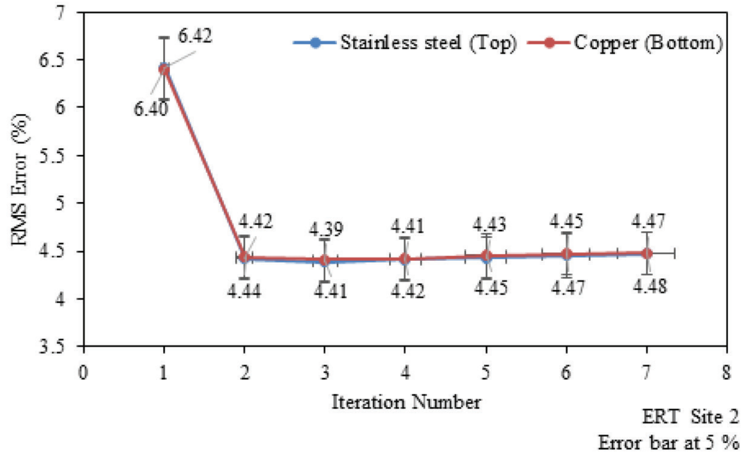

(b)

Figure 8: (Continue).

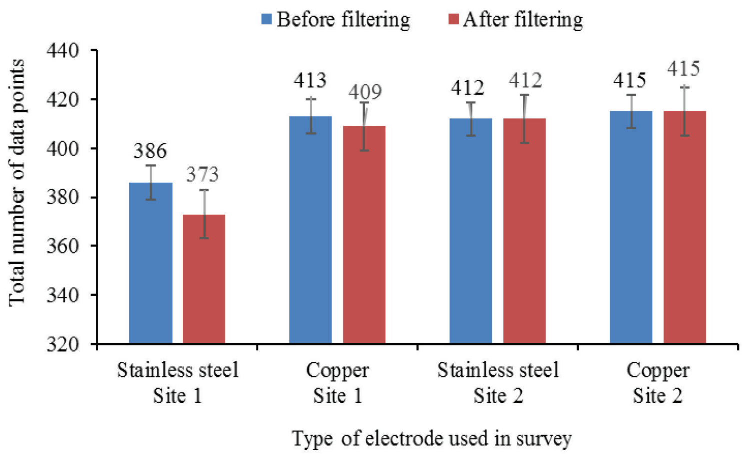

Figure 9: Comparative analyses of the total number (population) of positive data points before filtering (blue bars) and after filtering (red bars) from both sites.

On the other hand, the RMS errors of the IP inversion models for stainless-steel and copper electrodes for both sites were significant with a large percentage relative difference for each iteration number (Figure 10) and were considerably lower than that observed for the ERT method. At Site 1, the RMS errors of the IP model reduced from 6.23% to 5.88% for the stainless-steel electrodes and 1.97% to 1.68% for the copper electrodes. Therefore, the relative differences in RMS errors also reduced from 4.26% to 4.20%. At Site 2, the RMS errors of the IP model reduced from 0.47% to 0.46% for the stainless-steel electrodes and from 0.21% to 0.18% for the copper electrodes. These results agree with the interpretation of the comparative analyses of positive population data points in Appendix 2.

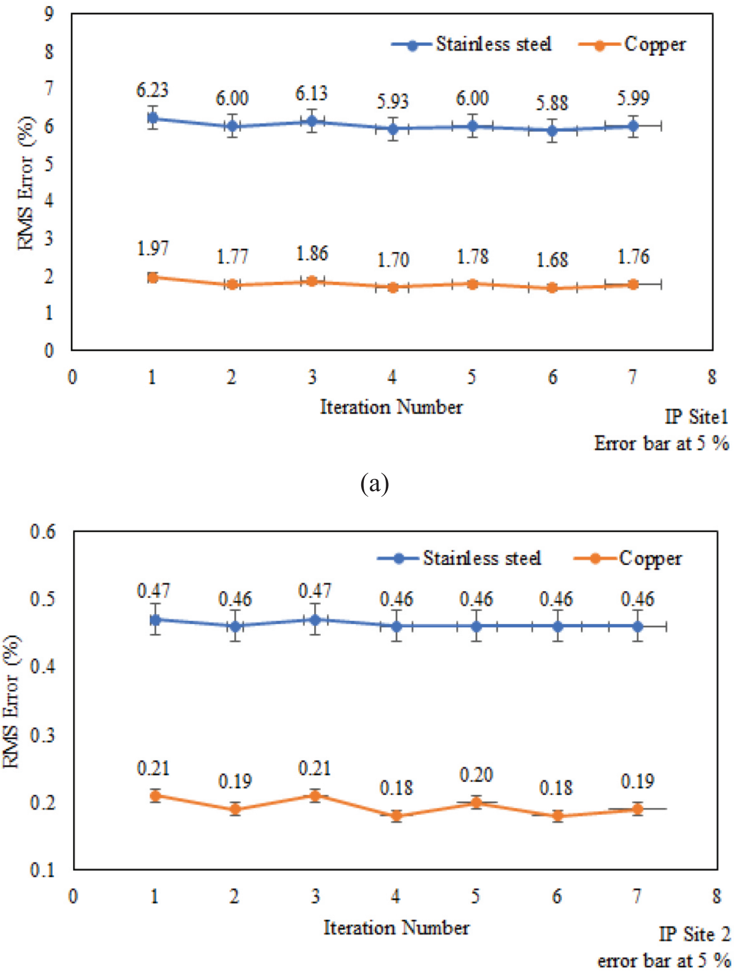

(a)

(b)

Figure 10: Graphs of RMS error versus iteration number of IP inversion models at (a) Site 1 and (b) Site 2.

Figure 11 presents the percentage relative differences between the ERT and IP inversion results for the conventional stainless-steel and copper electrodes. The findings indicated that the ERT and IP inversion results from Site 1 yielded a range of percentage relative differences of –70% to 70% (Figure 11). This range demonstrated a striking difference between the recorded datasets population using the two electrodes. Moreover, the statistical analyses, which evaluated the performances between the electrodes for all data points, derived population μ values of 14.46% and 12.67% for the ERT and IP inversion models at Site 1, with population SD (σ) values of 31.91% and 44.74% and population RMS errors of 35.03% and 46.50% of data points, respectively. These statistical results exhibited large variations in recorded geophysical parameters (resistivity and chargeability) using these two electrodes, especially due to the high SD and high RMS errors with values above 30%. For Site 1, the population MAPE values of ERT and IP inversion models were 28.69% and 40.25% of data points, respectively. It has affirmed that stainless-steel electrodes are capable to provide reasonable forecast accuracy for both resistivity and chargeability data.[2,21]

Figure 12, on the other hand, illustrates the relative differences between the copper and conventional stainless-steel electrodes for Site 2, with values ranging between –8% and 8%. This range demonstrated a significant contrast (about 10 times lower) between their percentage relative differences obtained at Site 1 for ERT and IP surveys. The population mean, μ values for ERT and IP inversion models were –0.33% and 0.48%, with population SD, σ of 2.80% and 3.67%, and population RMS errors of 2.82% and 3.70% of data points, respectively. Lastly, the population MAPE values for ERT and IP inversion models were 2.19% and 3.06% of data points, respectively. It shows that the small unit electrode spacing of stainless-steel will provide highly accurate forecast in both resistivity and chargeability data.[2,21] These statistical results have revealed that a small unit electrode spacing of 2.5 m can yield better voltage decay results. Hence, the copper electrode is a good conductor of electric current to be used in ERT and IP surveys compared to the conventional stainless-steel electrodes. In general, the results of this study provided additional and detailed clues that the choice of electrode selection is a pertinent factor for attenuating noise and improving the efficiency and resolution of the electrical tomographic models for subsurface characterisation at larger spatial and temporal scales as suggested by some researchers.[9,10,18]

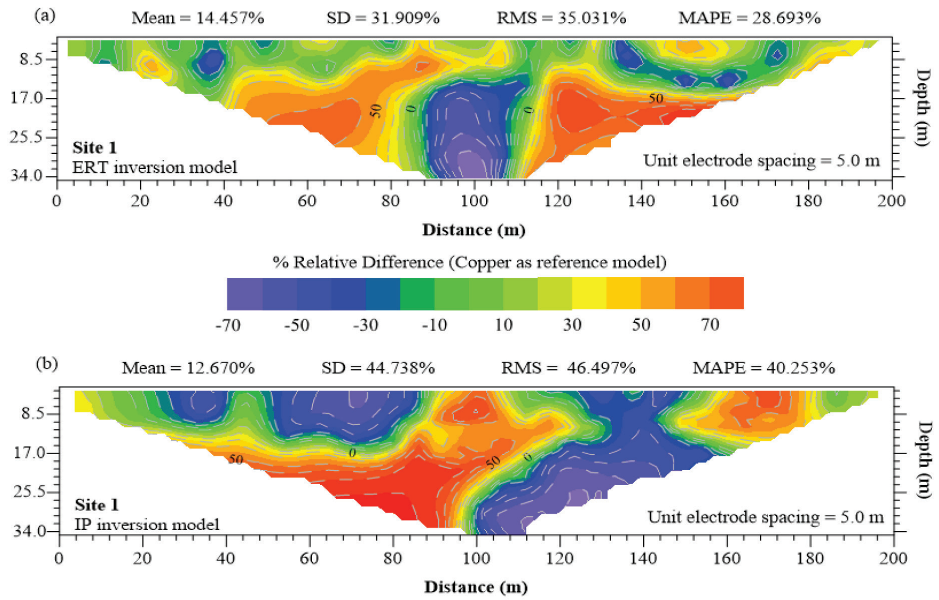

Figure 11: Percentage relative differences between copper and conventional stainless-steel electrodes in (a) ERT and (b) IP inversion models from Site 1.

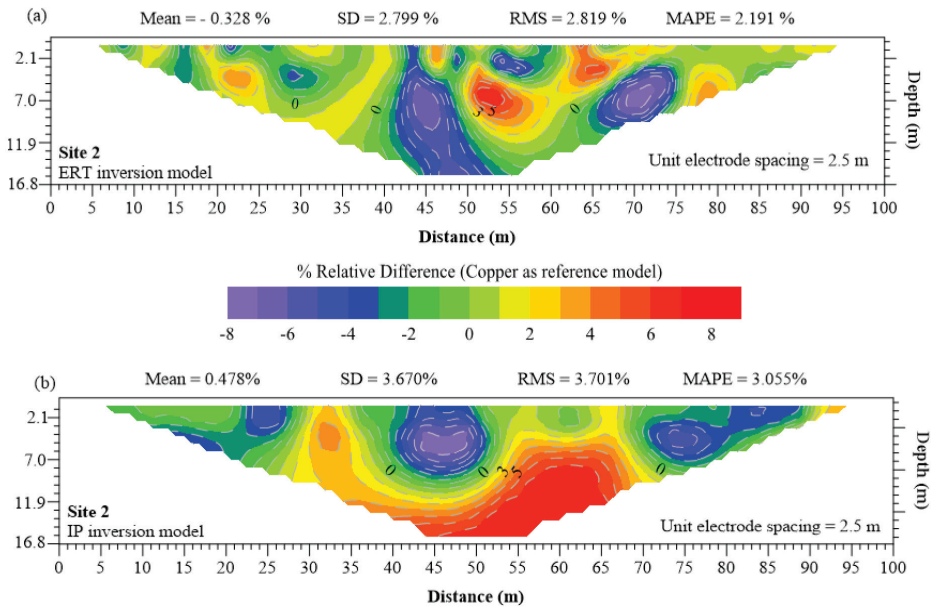

Figure 12: Percentage relative differences between copper and conventional stainless-steel electrodes in (a) ERT and (b) IP inversion models from Site 2.

5. CONCLUSION

Based on the obtained results in this study, we have indicated significant subsurface information using the quality of data points, iteration levels, and RMS errors as criteria to evaluate the performance of stainless-steel and copper electrodes in ERT and IP tomographic surveys. The analyses of data quality indicated a striking difference between the spacing of two different electrodes in ERT and IP surveys. It shows that copper as a non-polarisable electrode is indispensable for an electrical survey requiring precise and sensitive measurement. Therefore, it could be concluded that large electrode spacing and survey lines in ERT and IP surveys require good electrical conductivity and non-polarisable electrodes; in this case, copper produced good inversion models compared to conventional stainless-steel electrodes. In addition, the inversion models using copper electrodes are more reliable due to the low RMS error values generated. Lastly, statistical results of population MAPE confirmed that stainless-steel electrodes are capable to provide reasonable forecast accuracy for ERT and IP inversion models (28.69% and 40.25%, respectively) for a unit electrode spacing of 5.0 m.

6. ACKNOWLEDGEMENTS

The first author expresses his gratitude to Adekunle Ajasin University and the Tertiary Education Trust Fund, Nigeria for providing financial support. The authors greatly appreciate all the comments and suggestions from the Editor-in-Chief and the anonymous reviewers, which have contributed enormously to the manuscript's quality and increased its readability.

7. REFERENCES

1. Dahlin, T., Leroux, V. & Nissen, J. (2002). Measuring techniques in induced polarization imaging. *J. Appl. Geophys.*, 50(3), 279–298. https://doi.org/10.1016/S0926-9851(02)00148-9
2. Balarabe, B. & Bery, A. A. (2021). Modeling of soil shear strength using multiple linear regression (MLR) at Penang, Malaysia. *J. Eng. Res.*, 9(3), 40–51. https://doi.org/10.36909/jer.v9i3A.7675
3. Mashhadi, S. R. & Ramazi, H. (2018). The application of resistivity and induced polarization methods in identification of Skarn Alteration Haloes: A case study in the Qale-Alimoradkhan area. *J. Environ. Eng. Geophys.*, 23(3), 363–368. https://doi.org/10.2113/JEEG23.3.363
4. Song, S.-H. et al. (2020). Delineation of leachate pathways using electrical methods: Case history on a waste plaster landfill in South Korea. *Explor. Geophys.*, 51(3), 301–313. https://doi.org/10.1080/08123985.2019.1700109

5. Mashhadi, S. R., Nikfarjam, M. & Mehrnia, A. K. (2020). Reinterpretation of resistivity and induced polarization data to explore gold mineralization zones at Zarzima prospect, Iran. *Acta Geol. Slovaca*, 12(1), 15–22.
6. Slater, L. & Lesmes, D. (2002). IP interpretation in environmental investigations. *Geophys.*, 67(1), 77–88. https://doi.org/10.1190/1.1451353
7. Slater, L. D. & Glaser, D. R. (2003). Controls on induced polarization in sandy unconsolidated sediments and application to aquifer characterization. *Geophys.*, 68(5), 1547–1558. https://doi.org/10.1190/1.1620628
8. Loke, M. H. (2004). Rapid 2D resistivity and IP inversion using the least-square method. Manual for RES2DINV (version 3.54). Penang, Malaysia: Geotomo Software Sdn Bhd.
9. LaBrecque, D. & Daily, W. (2008). Assessment of measurement errors for galvanic-resistivity electrodes of different composition. *Geophys.*, 73(2), F55–F64. https://doi.org/10.1190/1.2823457
10. Daily, W. et al. (2005). Electrical resistance tomography: Theory and practice. In D. K. Butler (Ed.), *Near surface geophysics (Investigation in geophysics no. 13)* pp. 525–550. Tulsa, Oklahoma, USA: Society of Exploration Geophysicists. https://doi.org/10.1190/1.9781560801719.ch17
11. Griffiths, D. J. (2017). *Introduction of electrodynamics*, 4th ed. Cambridge University Press: Cambridge, UK. https://doi.org/10.1017/9781108333511
12. Clark, A. F., Childs, G. E. & Wallace, G. H. (1970). Electrical resistivity of some engineering alloys at low temperatures. *Cryogenics*, 10(4), 295–305. https://doi.org/10.1016/0011-2275(70)90056-1
13. Ong, W. S. (1993). *The geology and engineering geology of Pulau Pinang. Geological survey of Malaysia, Map report*. p 7. Kuala Lumpur: Jabatan Penyiasatan Kajibumi Malaysia.
14. Ahmad, F., Yahaya, A. S. & Farooqi, M. A. (2006). Characterization and geotechnical properties of Penang residual soils with emphasis on landslides. *Am. J. Environ. Sci.*, 2(4), 121–128. https://doi.org/10.3844/ajessp.2006.121.128
15. Abdul Hamid, F. A. Z. et al. (2019). Distribution and contamination assessment of potentially harmful elements (As, Pb, Ni, Cd) in top soil of Penang Island, Malaysia. *Environ. Earth Sci.*, 78(21), 616–627. https://doi.org/10.1007/s12665-019-8626-0
16. deGroot-Hedlin, C. & Constable, S. C. (1990). Occam's inversion to generate smooth two-dimensional models from magnetotelluric data. *Geophys.*, 55(12), 1613–1624. https://doi.org/10.1190/1.1442813
17. Scapozza, C. & Laigre, L. (2014). The contribution of electrical resistivity tomography (ERT) in Alpine dynamics geomorphology: Case studies from the Swiss Alps. *Geomorphol. Relief, Process. Environ.*, 20(1), 27–42. https://doi.org/10.4000/geomorphologie.10474
18. Akingboye, A. S. & Ogunyele, A. C. (2019). Insight onto seismic refraction and electrical resistivity tomography techniques in subsurface investigation. *The Min-Geol-Petrol. Eng. Bull.*, 34(1), 93–111. https://doi.org/10.17794/rgn.2019.1.9

19. Sirhan, A., Hamidi, M. & Andrieux, P. (2011). Electrical resistivity tomography, an assessment tool for water resource: A case study of Al-Aroub Basin, West Bank, Palestine. *Asian J. Earth Sci.*, 4(1), 38–45. https://doi.org/10.3923/ajes.2011.38.45
20. Cardarelli, E. & Di Filippo, G. (2009). Electrical resistivity and induced polarization tomography in identifying the plume of chlorinated hydrocarbons in sedimentary formation: A case study in Rho (Milan – Italy). *Waste Manag. Res.*, 27(6), 595–602. https://doi.org/10.1177/0734242X09102524
21. Abidin, S. N. Z. & Jaffar, M. M. (2014). Forecasting share prices of small size companies in Bursa Malaysia using Geometric Brownian Motion. *App. Math. Inf. Sci.*, 8(1), 107–112. https://doi.org/10.12785/amis/080112